

A flow adaptive aerodynamic probe concept for turbomachinery

To cite this article: C Lenherr *et al* 2007 *Meas. Sci. Technol.* **18** 2599

View the [article online](#) for updates and enhancements.

Related content

- [Time-resolved flow measurements with fast-response aerodynamic probes in turbomachines](#)
- [Time-resolved entropy measurements using a fast response entropy probe](#)
- [An optical backscatter probe for time resolved droplet measurements in turbomachines](#)

Recent citations

- [Quasi Two-Dimensional Flow-Adaptive Algorithm for Pneumatic Probe Measurements](#)
Christian Bartsch *et al*
- [One-Dimensional Flow-Adaptive Measurement Grid Algorithm for Pneumatic Probe Measurements](#)
Christian Bartsch *et al*
- [Design Considerations for Axial Steam Turbine Rotor Inlet Cavity Volume and Length Scale](#)
Konstantinos G. Barmalias *et al*

A flow adaptive aerodynamic probe concept for turbomachinery

C Lenherr, A I Kalfas and R S Abhari

Turbomachinery Laboratory (LSM), Swiss Federal Institute of Technology, ETH Zurich, CH-8092 Zurich, Switzerland

E-mail: lenherr@lsm.iet.mavt.ethz.ch

Received 6 September 2006, in final form 30 April 2007

Published 11 July 2007

Online at stacks.iop.org/MST/18/2599

Abstract

A flow adaptive 2D traversing algorithm is developed and demonstrated with measurements in a large axial turbine facility. This novel approach is suited for pneumatic probe and fast response aerodynamic probe measurements. The implementation of the algorithm is fully automated and requires a minimal input, such as blade count and hub and tip diameters, at set-up. The algorithm automatically selects measurement points, such as shear flows, secondary flows, wakes through user-defined detection functions, and adds additional measurement points; therefore higher measurement fidelity in these regions is obtained compared to a traditional measurement method. The flow adaptive 2D traversing algorithm can resolve the overall flow field with 75% fewer measurement points compared to a uniform a measurement grid. This reduction in measurement points results in a measurement time using the flow adaptive algorithm that is 81% quicker than on a uniform measurement grid, without loss of measurement accuracy.

Keywords: adaptive traversing, aerodynamic probe measurement, turbomachinery

(Some figures in this article are in colour only in the electronic version)

Nomenclature

C_{pt}	total pressure coefficient	$\frac{P_{tot} - P_{stat,exit}}{P_{tot,inlet} - P_{stat,exit}}$	(–)
M	Mach number	(–)	
P_{atm}	atmospheric pressure	(Pa)	
P_{stat}	static pressure	(Pa)	
P_{tot}	total pressure	(Pa)	
α	flow yaw angle	(deg)	
β	flow pitch angle	(deg)	
d	distance	(m)	
\bar{v}	velocity vector	(m s ⁻¹)	

Subscripts

i	index, counter
x	axial direction
θ	circumferential
r	radial

Abbreviations

D	dimensional
DF	detection function
FP	flow property value
N_L	number of loops
N_P	number of points/loop
N_T	total number of possible measurement points
N_A	actual number of measurement points
PG	pressure gradient section
PM	minimal pressure section
PS	blade pressure side
SS	blade suction side
TC x	test case no x
YA	yaw angle section

1. Introduction

The measurement, analysis and prediction of detailed flowfield features, such as wakes and vortices, are major issues

in the development of modern turbomachinery designs. Furthermore, an understanding of the complex physical processes associated with these flow phenomena is required to improve the efficiency and performance of turbomachinery. In the past two decades computational fluid dynamic methods (CFD) have played an increasingly important role in the design of modern turbomachinery design, especially for reasons related to development costs. However, CFD methods are still limited by available computing power in particular when unsteady flows must be resolved. There are also a number of issues related, for example, to turbulence or subgrid modelling, numerical accuracy and or boundary conditions that remain unresolved. Thus the role of experimental measurement techniques shall remain important for the foreseeable future.

Sieverding *et al* [1] provide a recent overview of measurement techniques for the unsteady flows in turbomachinery applications. Due to the harsh environment and limited accessibility of turbomachinery, point measurements derived from intrusive probes are the bulk of techniques used in industrial applications. In the industrial setting, a substantial amount of time, money and effort is expended in setting up, conducting, reducing and analysing the large volumes of data that derive from point measurements. There is therefore great interest in the reduction of the required time for turbomachinery tests, as these reduce development costs and maintain competitiveness [2].

We present here a novel flow adaptive traversing algorithm that has been used with both pneumatic and fast response probes [3]. This algorithm requires minimal user input at the outset, thus reducing the set-up time for a measurement campaign. During the measurements, in an automated manner, the algorithm detects and measures flow features such as wakes and regions of secondary flows, such as vortical structures. This automated adaptation of flow measurement regions is important as regions in which measurements must be performed are not always intuitive. For example, in blade row clocking the flow phenomena of interest move with respect to the stationary frame of reference; this movement is not always proportional to the clocking angle [4]. In this case, the flow adaptive algorithm yields measurements at points related to the actual flow field, and thus the result with different clocking angles can be compared in an unbiased fashion. The number of measurement points on the flow-adapted grid is substantially reduced compared to a uniform grid, without a loss of measurement accuracy. Thus the measurement time and the time for data reduction are reduced; also there are savings in the electronic space required to store the data.

The format of the paper is as follows. First, the flow adaptive traversing algorithm is described. Then the instrumentation and axial turbine facility that are used to demonstrate the algorithm are presented. Measurements of the total pressure coefficient and yaw angle on uniform and flow-adapted measurement grids at the second stator exit are then discussed. The paper then concludes with a summary of significant contributions of this new development.

2. Flow adaptive traversing algorithm

The flow adaptive algorithm is designed to first detect points/areas of interest and then in an automated manner, add

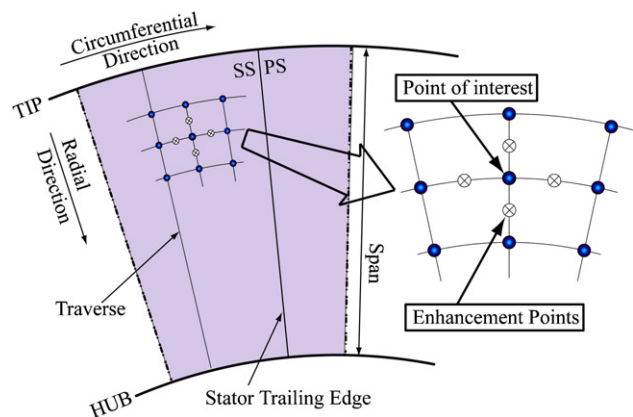


Figure 1. Illustration of new enhancement points added around a point of interest.

more measurement points. The adaptation is accomplished in both the radial and circumferential directions in the measurement plane (figure 1).

Three sequential steps—pre-processing, main processing and post-processing—constitute the flow adaptive algorithm.

2.1. Pre-processing

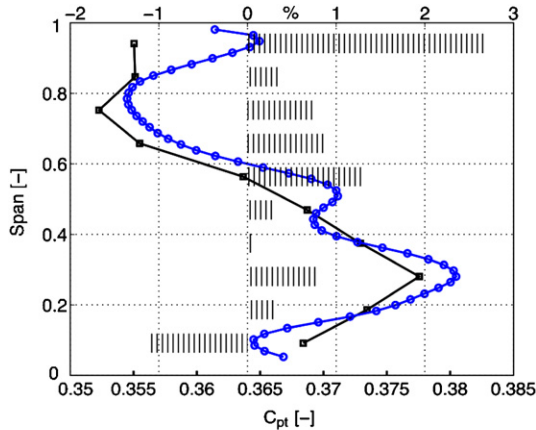
The first step in the flow adaptive method is to define an initial uniform grid of measurement points. This initial uniform grid must cover the whole measurement domain with an optimum number of points such that the measurement time is short and no important flow details are missed. Subsequent flow-adapted grids are based on this initial uniform grid. Algorithms that start from a uniform start grid to generate an adapted grid have been applied in adaptive mesh techniques for CFD [5]; thus in this regard the present approach is novel for measurement techniques but not new in fluid dynamics.

The optimum number of points to be used on the initial uniform grid was experimentally examined in the 2D axial measurement plane, figure 1, of the two-stage axial research turbine that is described below. This optimum number of points is a function of the geometrical parameters of the measurement plane, and thus will vary from one facility to another. For the present facility on the order of 10^2 (that is approximately 10×10 points in the circumferential and radial directions, respectively) were found to be optimal.

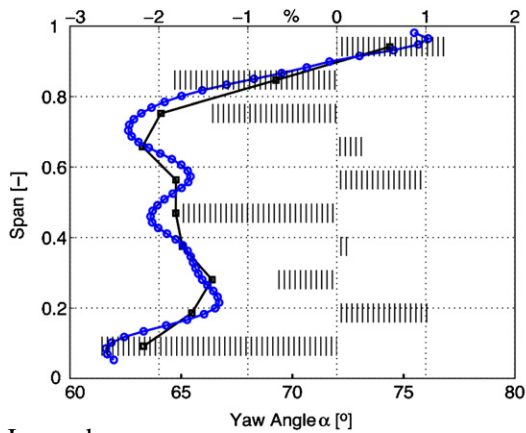
Typical spanwise profiles of the mass-averaged total pressure coefficient and yaw angle are shown in figure 2.

The profiles are shown for two grids, an initial uniform grid and a fine uniform grid. The initial uniform grid has 8×11 points and the latter grid has 45×59 points. This second grid is twice as dense in both radial and circumferential directions than a typical measurement grid that is used in the present facility without a flow adaptive measurement technique. In figure 2 the per cent difference between the profiles on the two grids is shown along the second x -axis. Overall the agreement between the profiles is very good, with the exception of the measured total pressure at the tip. In this case, the relatively coarse initial uniform grid does not capture the tip leakage effects. However, when we consider that the initial uniform grid has 30 times fewer measurement points (88 compared with 2655) than the fine uniform grid,

Spanwise distributions of circumferentially mass averaged total pressure coefficients and deviation between the results



Spanwise distributions of circumferentially mass averaged yaw angles and deviation between the results



Legend:
—●— Fine Uniform Grid 45 x 59
—■— Initial Uniform Grid 8 x 11
||||| Deviation in %

Figure 2. Comparison of spanwise distributions of circumferentially mass-averaged C_{pt} and yaw angles on a fine uniform grid and initial uniform grid. The second x -axis shows the deviation between the two measurements.

the 1%–2.7% differences in the total pressure coefficient and 1.2%–2.7% differences in the yaw angle are very small.

After the initial uniform grid is specified, the pre-processing step is concluded with the definition of a finest uniform grid. Not all the points of this second grid are used; rather this second grid is used as the basis for an interpolated measurement grid when regions of interest are detected in the main processing step of the 2D adaptive algorithm. The desired measurement time and details of the probe geometry are amongst the parameters used, together with the initial uniform grid, to define this finest uniform grid.

2.2. Main processing

The refinement to a flow-adapted grid and measurements on this adapted grid are done during the main processing step. The refinement is based on user-defined detection criteria that identify regions of interest in the measurement plane.

In the present work detection criteria are specified, and thus the main processing step has three phases. In each phase a detection criterion is applied, the grid is refined and a series of measurements are made. In order to automate the main processing, the number of times to repeat a phase (termed here, loops), the number of points to be measured in each loop and termination criteria are specified *a priori*.

The termination criteria are based on user-specified minimum and maximum distances and the distances between a measurement point of interest and its neighbouring measured points. If the distance between the point of interest and a previously measured neighbouring point is not less than the user-specified minimum distance, then a new measurement point is inserted midway between the point of interest and the previously measured points. If the distance exceeds a user-specified maximum distance, then the newly inserted measurement point is placed at a specified distance from the point of interest. This procedure ensures that the new measurement points are within the area of interest; our experience shows that the overall quality of measurements on the flow-adapted grid is then better. The user-specified minimum and maximum distances are defined in terms of the positioning uncertainties of the probe traversing system and the diameter of the probe head.

The insertion of new measurement points results in an unstructured grid. However it is computationally more efficient to perform the data acquisition tasks on a structured grid using an object-oriented programming language. Thus after each refinement, the resulting unstructured grid is interpolated onto a structured utility grid. This structured grid has the same grid point spacing as that of the finest uniform grid. A distance weighed mean averaging procedure is used for the interpolation.

As described above, the adaptation of the grid and measurements are done in a series of phases. In each phase, a detection criterion is used as the basis for the adaptation. In the present work, the axial turbine flow, that is examined, is characterized by wakes, which are shed from the rotor and stator blades, and vortices that are generated by the passage and leakage flows. Thus three detection functions, minimum pressure (PM), pressure gradient (PG) and yaw angle (YA), are employed. The pressure-related functions provide for accurate measurements in the wake, since the total pressure in the wake is lower than that of its surrounding flow.

Kalfas *et al* [6] and Binder *et al* [7] have shown that the yaw angle is a reliable indicator to identify both wakes and vortices, especially in the passage downstream of a stator. Thus the sequence of detection, adaptation and measurement phases, figure 3, is PM, PG and finally YA.

In the PM phase, the adaptation and measurements are performed if local minima of the measured total pressures are found. In the PG and YA phases, the adaptation and measurements are performed if the detection functions exceed a threshold value. The detection functions for the pressure gradients are

$$DF_i(r) = \left(\frac{\partial P_{tot}}{\partial r} \right)_i^2 \quad (1)$$

$$DF_i(\theta) = \left(\frac{\partial P_{tot}}{\partial \theta} \right)_i^2 \quad (2)$$

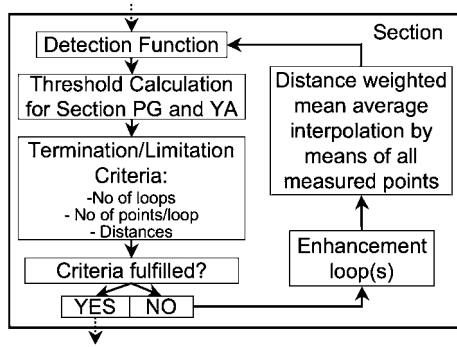


Figure 3. Flow chart of an adaptation and measurement phase.

And for the yaw angle

$$DF_{1i} = \left(\frac{\partial\alpha}{\partial r}\right)_i^2 \cdot \left(\frac{\partial\alpha}{\partial\theta}\right)_i^2 \quad (3)$$

$$DF_{2i} = \left(\frac{\partial^2\alpha}{\partial r^2}\right)_i^2 \cdot \left(\frac{\partial^2\alpha}{\partial\theta^2}\right)_i^2 \quad (4)$$

The threshold value is given as

$$\text{threshold} = \frac{1}{m} \cdot \sum_{i=1}^m DF_i, \quad (5)$$

where DF_i is a detection function given in equations (1)–(4). It is pertinent to point out that the detection functions involve squares of the first and second derivatives. This results in smoother distributions of the detection functions and improved identification of the points of interest.

2.3. Post-processing

The adaptation algorithm is initiated on the initial uniform starting grid, and then is applied on successively refined grids as areas of interest are identified and measured. If a uniformly spaced grid were used for the measurements, then the measurement data would be stored in matrices that are easily post-processed. However as the 2D flow adaptive algorithm results in measurements that are clustered in areas of interest, the resultant measurement data are not amenable to efficient post-processing. Thus the measurements on the flow-adapted grid are interpolated back onto a uniform grid in order to facilitate the post-processing. This interpolation is done in two steps. First, a 1D cubic spline is used to uniformly space points along the boundary of the measurement area. Then the flow parameters at each uniformly spaced point (x_0, y_0) are evaluated as a distance weighted average of the four closest measurement points. For example, for the yaw angle:

$$\alpha_{(x_0, y_0)} = \frac{\frac{\alpha_1}{d_1} + \frac{\alpha_2}{d_2} + \frac{\alpha_3}{d_3} + \frac{\alpha_4}{d_4}}{\sum_{i=1}^4 \frac{1}{d_i}} \quad (6)$$

3. Experimental validation of the technique

3.1. Instrumentation

Two probes, a pneumatic cobra-shaped five-hole probe [8], figure 4, and a fast response aerodynamic probe (FRAP)

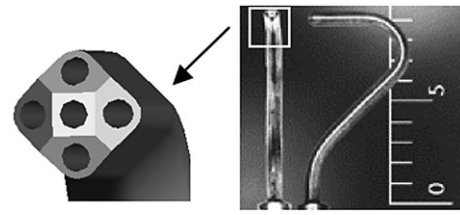


Figure 4. Cobra-shaped five-hole probe.

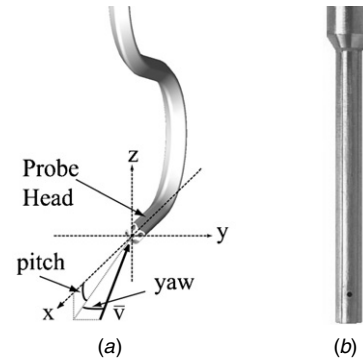


Figure 5. (a) Yaw and pitch angle convention; (b) fast response aerodynamic probe.

[9], figure 5, are used to evaluate the flow adaptation algorithm. Gossweiler *et al* [10] and Johansen *et al* [11] discuss the calibration procedures for the aforementioned probes. Traditional calibration techniques are limited to small flow angles [12], but a theoretical basis for extending the range of flow angles, beyond those used in the calibration, has been given by Pisasale *et al* [13]. The pneumatic probe has a calibration range of $\pm 12^\circ$ in the yaw angle and $\pm 30^\circ$ in the pitch angle (figure 5). The diameter of the probe head is 0.9 mm and the tip has a slanted pyramid shape (figure 4). The five-hole probe yields steady measurements of α , β , P_{tot} , P_{stat} and M .

Unsteady measurements are derived from the FRAP (figure 5(b), [10, 14–18]). This probe incorporates a single, temperature-compensated sensor that is operated using a Wheatstone bridge. The diameter of the cylindrical probe is 1.8 mm. The pressure tap is located 1.8 mm from the probe tip and has an angle of 0° with respect to the x -axis (figure 5(a)).

The sign convention is that a positive yaw angle is in the direction of the rotor sense of rotation (y -axis), and a positive pitch angle is directed towards the blade tip (z -axis).

3.2. Facility

The 2D adaptive flow concept was applied in the axial turbine research facility ‘LISA’ [19]. This is a large (max. power 400 kW), low speed (Mach numbers 0.1–0.4) facility that can accommodate up to two axial turbine stages. The primary characteristics of the turbine used in this study are given in table 1.

The present measurements are made in a traversing plane that is located downstream of the second stator row (figure 6).

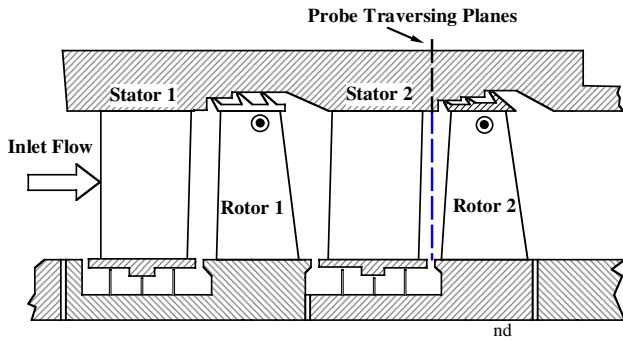


Figure 6. Measurement position after the second stator.

Table 1. Characteristic turbine parameters.

Parameter	Value
Rotational speed	2500 RPM
Pressure ratio	1.34
Aspect ratio (Span/Ax. Chord)	1.8
Blade count (Rotor/Stator)	42/42
Outer tip diameter	0.8 m
Mass flow	10.26 kg s ⁻¹

Table 2. Test case 1 (TC1).

Phase	N_L	N_P	N_T	N_A
Initial grid	1	88	88	88
PM	3	50	150	118
PG	2	40	80	64
YA	4	50	200	84

Table 3. Test case 2 (TC2).

Phase	N_L	N_P	N_T	N_A
Initial grid	1	88	88	88
PM	4	50	200	145
PG	4	40	160	133
YA	4	40	160	147

3.3. Test matrix

The baseline grid used to evaluate the 2D flow adaptive algorithm is a uniform grid with dimensions of 23×60 points in the circumferential and radial directions, respectively. Two test cases, TC1 and TC2, with flow-adapted grids are examined. The salient features of these grids are summarized in tables 2 and 3. The primary differences in the two test cases are the number of loops in the PM, PG and YA phases of the main processing step, and the number of measurement points in each of these loops.

The total numbers of possible measurement points are 518 and 608 for the test cases TC1 and TC2, respectively. However, due to the termination criteria based on distances that are discussed in section 2.2, the actual numbers of measurement points are 354 and 513, respectively, compared to 1380 points on the baseline uniform grid. In the subsequent section contour plots and circumferentially mass averaged line plots of the measured total pressure coefficients and yaw angles are presented for the two test cases to show the application of the 2D flow adaptive algorithm. In the contour plots, circle symbols that show the location of the measurement points

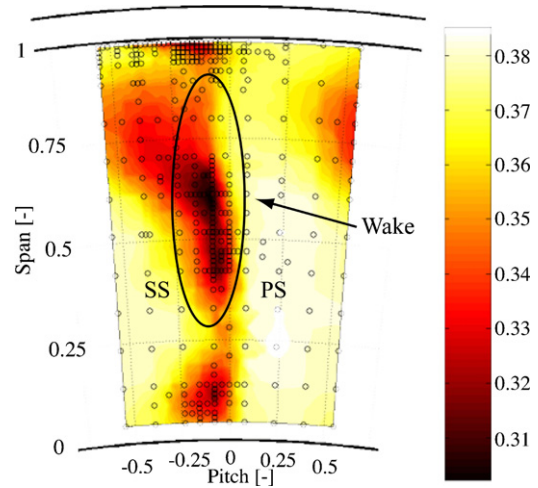


Figure 7. C_{pt} distribution for test case TC1.

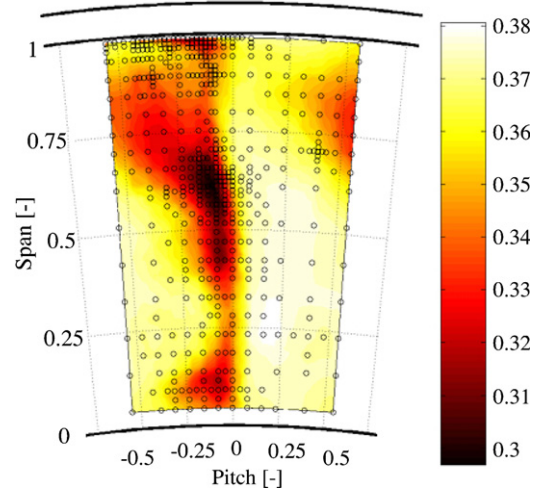


Figure 8. C_{pt} distribution for test case TC2.

are superposed on the flowfield contours. Although other flow variables could be shown on the plots, the total pressure and yaw angle are presented since they are also used in the detection functions.

3.4. Discussion of results

Figures 7 and 8 show contours of the total pressure coefficients at the end of the measurement series for test cases TC1 and TC2, respectively. Since a five-hole probe and FRAP are used for the measurements, a safety clearance must be maintained close to the hub. Additionally near the rotor tip, there is a leakage flow that results in yaw angles that are outside the calibration range of the probe. Thus in figures 7 and 8, and in the subsequent contour plots, the regions in the range of 0–5% span and 99–100% span are shown as blanked out white zones.

A comparison of test case TC1, figure 7, to test case TC2, figure 8, shows that although the former has approximately 30% fewer measurement points, there are no significant differences between the two cases.

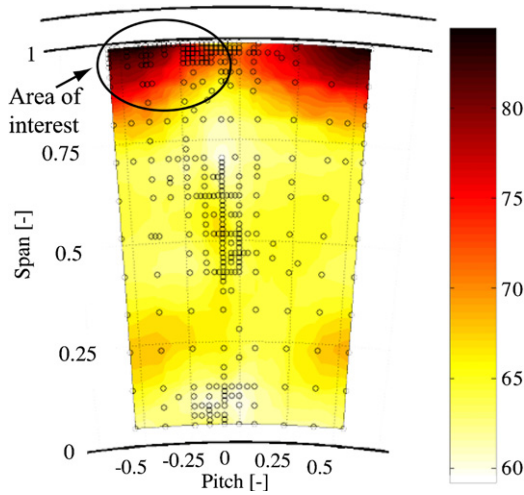


Figure 9. Yaw angle α (deg) distribution for test case TC1.

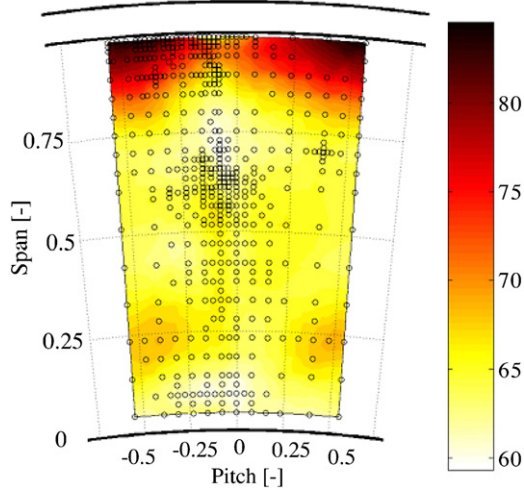
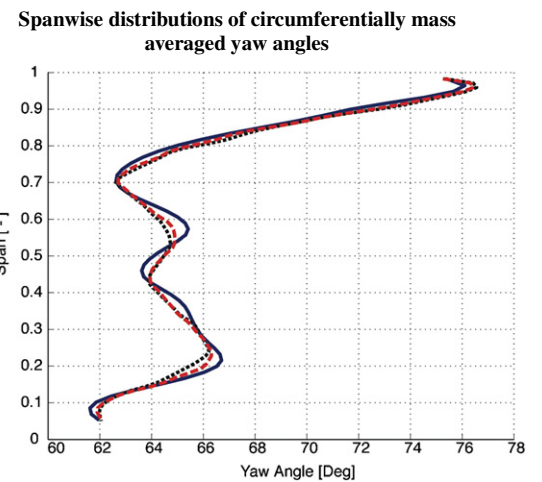
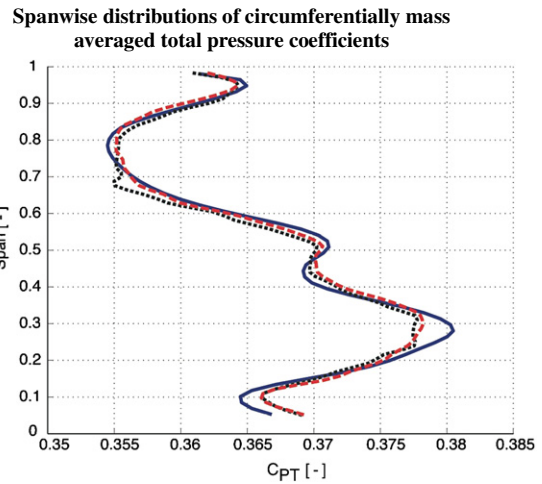


Figure 10. Yaw angle α (deg) distribution for test case TC2.

This is confirmed in figure 11 where the spanwise distributions of the circumferentially mass-averaged total pressure coefficient and yaw angle are shown, and compared to those of the reference grid. It can be seen from the circle symbols in figures 7 and 8 that the 2D flow adaptive algorithm results in more finely resolved measurements in the regions of low total pressure that are associated with the wake. For test case TC2, table 3, more loops involving the pressure-related criteria are performed in comparison to the test case TC1, table 2. Thus a comparison of figures 7 and 8 also shows that test case TC2 has a higher density of measurement points in the wake and its surrounding flow. This higher density of measurement points is also evident when the yaw angles are compared in figures 9 and 10.

Figures 9 and 10 also show that there is a relatively high density of measurement points in the outer 25% span of the measurement plane. In this region the tip leakage vortex results in relatively high gradients of the yaw angle.

A close-up view of the measured total pressure and yaw angles is shown in figures 12–17. In these contour plots only the outer 50% span is shown for the uniform grid and the two



Legend:
 — Fine Uniform Grid 45 x 59
 Adaptive Test Case TC1
 - - - Adaptive Test Case TC2

Figure 11. Comparison of spanwise distributions of circumferentially mass-averaged C_{pt} and yaw angles on a fine uniform grid and grids of adaptive test case TC1 and adaptive test case TC2.

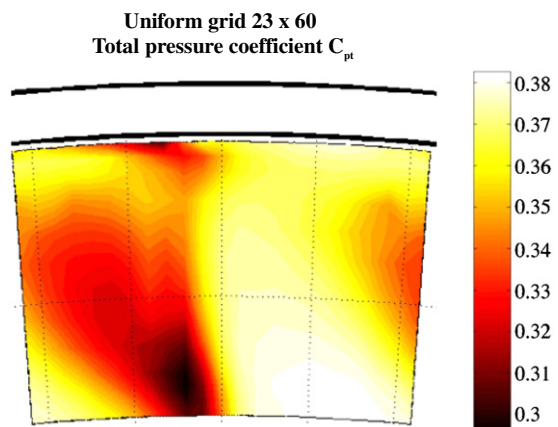


Figure 12. Upper 50% span of C_{pt} distribution over one pitch measured on the uniform grid 23x60.

test cases, TC1 and TC2. The total pressure coefficients are shown in figures 12–14 and the yaw angles in figures 15–17.

Flow adaptive probe concept
Total pressure coefficient C_{pt} , TC1

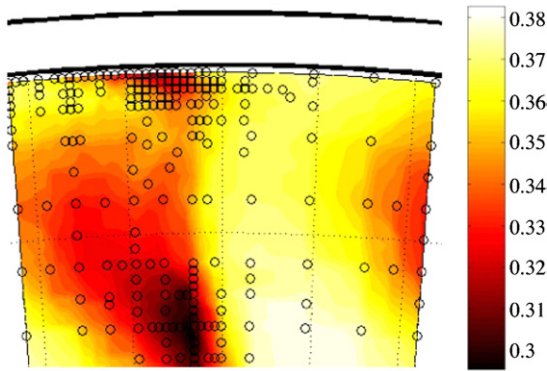


Figure 13. Upper 50% span of C_{pt} distribution over one pitch measured on the flow-adapted grid, TC1.

Flow adaptive probe concept
Yaw angle α , TC1

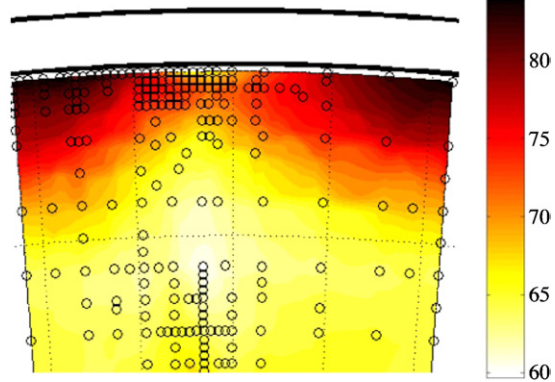


Figure 16. Upper 50% span of α (deg) distribution over one pitch measured on the flow-adapted grid, TC1.

Flow adaptive probe concept
Total pressure coefficient C_{pt} , TC2

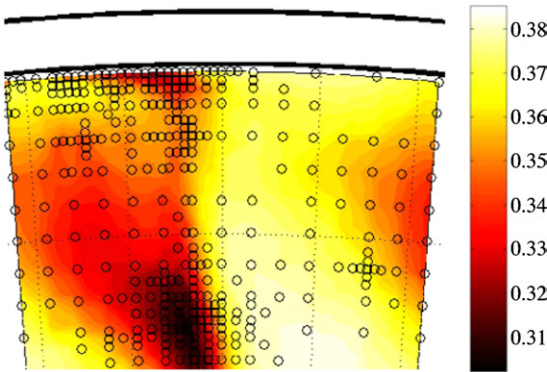


Figure 14. Upper 50% span of C_{pt} distribution over one pitch measured on the flow-adapted grid, TC2.

Flow adaptive probe concept
Yaw angle α , TC2

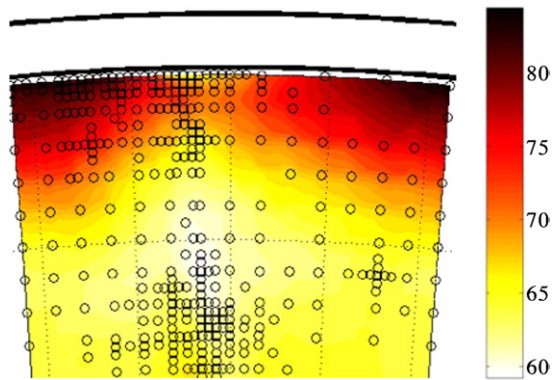


Figure 17. Upper 50% span of α (deg) distribution over one pitch measured on the flow-adapted grid, TC2.

Uniform grid 23 x 60
Yaw angle α

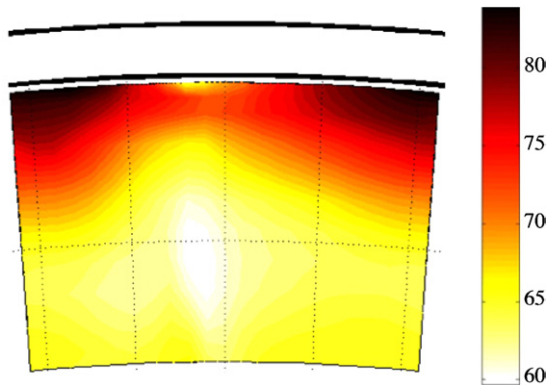


Figure 15. Upper 50% span of α (deg) distribution over one pitch measured on the uniform grid 23 x 60.

Overall it can be seen that there is very good qualitative agreement between the two flow-adapted grid test cases and the reference case. As described above, more highly refined measurements are obtained at around 60% span in the vicinity of the wake, and around 90% span in the region of the tip leakage flow. Although there is a high density of measurement

points in these two regions, a comparison of for example figure 16 (test case TC1) and figure 17 (test case TC2) shows that there are measurement points distributed over the whole measurement plane. The user-specified minimum spacing distance assures that additional points are not inserted in the regions of interest, even if the number of measurement loops is high. The small differences between the flow-adapted results, figures 13, 14, 16 and 17, compared to the reference case, figures 12 and 15, are thought to be a result of the non-uniform grid in the flow-adapted test cases and the uniform grid in the reference case. The measurements on the non-uniform grid have to be interpolated back onto a uniform grid during the data processing step described above. It is thought that the use of a higher order interpolation scheme would minimize these differences. Nevertheless, the spanwise distributions of the circumferentially mass-averaged total pressure coefficients and yaw angles, shown in figure 11, show that the differences between the flow-adapted grid and uniform grid are small.

The measurement times for the three cases are 8 h for the uniform grid, 1.5 h for test case TC1 and 3 h for test case TC2. The difference in the measurement times on the flow-adapted grids is a result of the difference in the number of measurement points, 354 points for test case TC1 compared

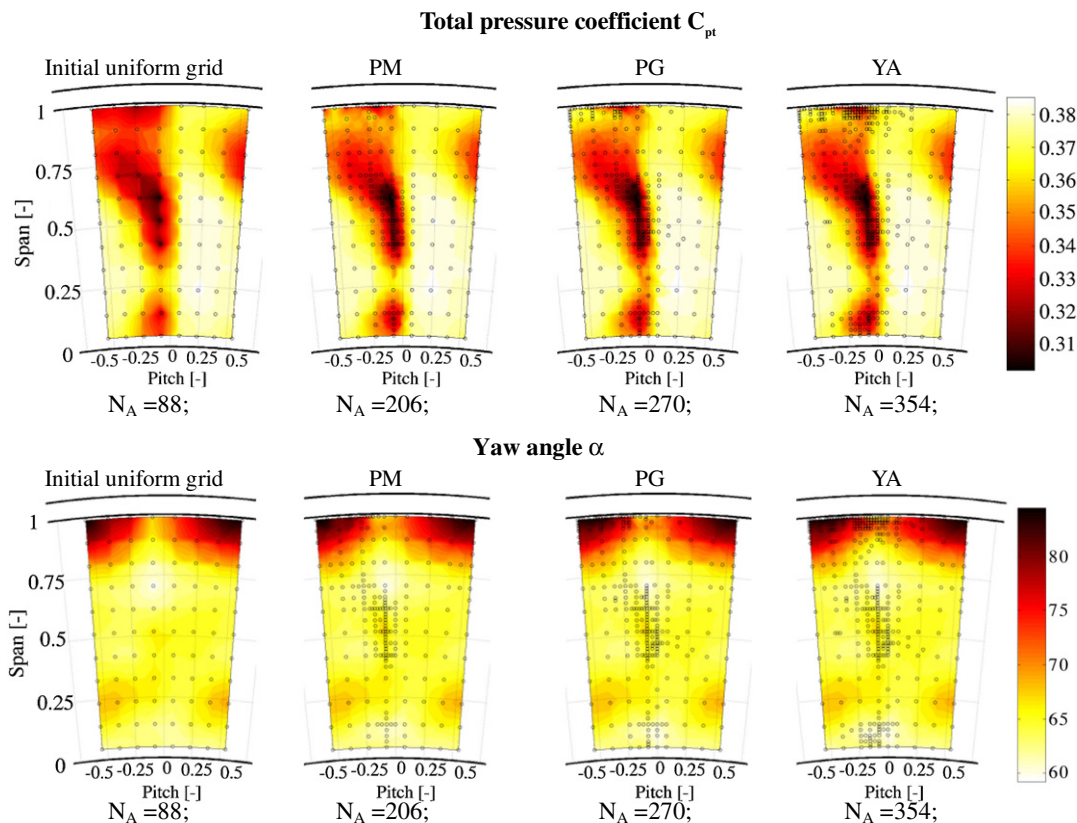


Figure 18. Evolution of C_{pt} and α (deg) distributions over one pitch during a run. Test case TC1.

to 513 points for test case TC2. Test case TC1 thus has a gain of 81% in measurement time compared to the uniform grid of the reference case.

The evolution of the grid adaptation during a series of measurements is shown in figure 18. Test case TC1 is shown as a representative example. In figure 18 the measured flowfield on the initial uniform grid, and then at the end of the three successive main processing phases, PM, PG and YA, are shown. The corresponding evolution of the mass-averaged total pressure coefficient and yaw angle is shown in figures 19 and 20. An error bar shows the uncertainty in the five-hole probe measurements and the result from the uniform grid is shown as a horizontal dashed line that is denoted as the trendline. It can be seen that 300 measurement points on the flow-adapted grid yield the same result (within the measurement uncertainty) as on the uniform grid that has 1380 points.

4. Further applications of the method

The applications of the novel flow adaptive algorithm are not limited to the test case considered above. Below we briefly summarize two other related applications.

4.1. Fast response aerodynamic probe (FRAP)

An accurate assessment of the losses in turbomachines requires the measurement of the unsteady flow field [20–22]. These measured flow properties can then be used to derive

Trend for changes in mass averaged C_{pt}

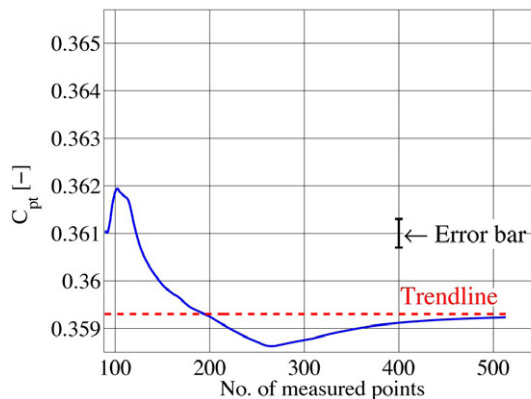


Figure 19. Evolution of the mass-averaged total pressure coefficient C_{pt} .

parameters such as the non-deterministic pressure coefficient and turbulence intensity that are used to quantify the losses. The initial development of the novel flow adaptive algorithm used the FRAP from which the aforementioned parameters can be determined. It is thus evident that the novel flow adaptive algorithm has the potential to facilitate the design and development of new turbomachines.

4.2. 1D flow adaptive traversing algorithm

The novel flow adaptive algorithm has been applied to a 1D radial traverse. In this case, the algorithm was used to

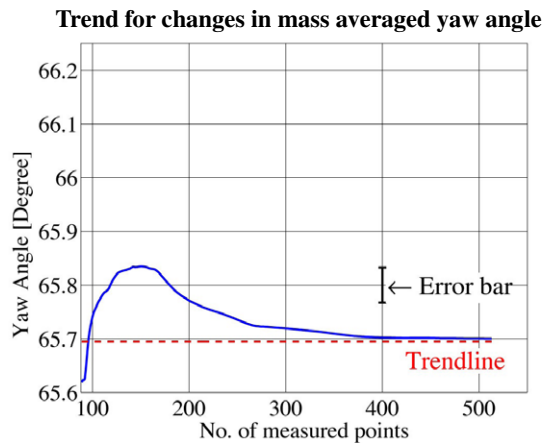


Figure 20. Evolution of the mass-averaged yaw angle α (deg).

automatically traverse a probe step-by-step from tip to hub. At each radial position, the previously acquired yaw angle α is used as an input for the following traverse point. After a traverse, points of interest are determined, and arrays of locally refined radial positions are generated. The measurement and refinement steps are repeated until the algorithm terminates due to the limitation criteria. Compared to measurement on a standard uniform grid without refinement, the 1D algorithm is 30% faster. As a 1D traverse is made, the detection functions in the circumferential direction are not evaluated. Therefore, the flow adaptive algorithm can be applied in test facilities in which an automated traverse in the circumferential direction is not available, since each radial traverse can be independently made.

5. Conclusions

A novel flow adaptive 2D traversing algorithm has been developed. Measurements in a large axial turbine facility demonstrate the potential of the algorithm to substantially reduce measurement time, whilst maintaining measurement accuracy. This novel approach can be used for pneumatic probe measurements, as well as for unsteady measurements using a fast response aerodynamic probe.

The flow adaptive algorithm is comprised of three sequential steps—pre-processing, main processing and post-processing. In the first step an initial uniform grid of points is defined and the flow is measured. Then in the next step, in an automated manner, the algorithm detects points/areas of interest, and adds additional measurement points as required. The adaptation is accomplished in both the radial and circumferential directions in the measurement plane. The detection functions employed in the present work identify the wakes, which are shed from the rotor and stator blades, and the vortices, that are generated by the passage and leakage flows. In the final step, the measurements on the flow-adapted grid are interpolated back onto a uniform grid in order to facilitate the post-processing.

The application of the flow adaptive 2D traversing algorithm shows that compared to a uniform measurement grid, a flow-adapted grid with 75% fewer measurement points

can be used to resolve the flow field. This reduction in measurement points has a significant impact on the measurement time; specifically measurement time using the flow adaptive algorithm is 81% quicker than on the uniform measurement grid. This measurement time is expected to be even further reduced in a 3D adaptive flow concept that is presently under development.

Acknowledgments

The authors would like to express their gratitude to the technical support personnel of the Turbomachinery Laboratory, and in particular to Cornel Reshef for his help and advice in the numerous electronic engineering issues that arose during the course of the algorithm development. Thanks are also due to Thomas Behr and Luca Porreca for the installation and the operation of the axial turbine research facility LISA.

References

- [1] Sieverding C H, Arts T, Dénos R and Brouckaert J F 2000 Measurement techniques for unsteady flows in turbomachines *Exp. Fluids* **28** 285–321
- [2] Franken A R C and Ivey P C 2002 Reducing aero-engine development time and costs by using artificial intelligence *22nd AIAA Aerodynamic Measurement Technology and Ground Testing Conf. (St. Louis, Missouri) AIAA Paper 2002-3251*
- [3] Lenherr C, Oschwald M, Kalfas A I and Abhari R S 2004 Flow adaptive aerodynamic probe for turbomachinery flows *17th Symp. on Measuring Techniques in Transonic and Supersonic Flows in Cascades and Turbomachines (Stockholm, Sweden)*
- [4] Behr T, Porreca L, Mokulys T, Kalfas A I and Abhari R S 2004 Multistage aspects and unsteady effects of stator and rotor clocking in an axial turbine with low aspect ratio blading *ASME Turbo Expo (Vienna) ASME Paper GT 2004-53612*
- [5] Thompson J F, Soni B K and Weatherill N P 1998 *Handbook of Grid Generation* (Boca Raton, FL: CRC Press)
- [6] Kalfas A I and Elder R L 1995 Determination of the intermittency distribution in the boundary layer of a flat plate with c4 leading edge *ERC OFTAC Bul. Transist.* **24** 65–7
- [7] Binder A and Romey R 1983 Secondary flow effects and mixing of the wake behind a turbine stator *ASME J. Turbomach.* **105** 40–6
- [8] Treiber M, Kupferschmied P and Gyarmathy G 1998 Analysis of error propagation arising from measurements with a miniature pneumatic 5-hole probe *Proc. 14th Symp. on Measuring Techniques for Transonic and Supersonic Flows in Cascades and Turbomachines (Limerick, Ireland)*
- [9] Schlienger J, Pfau A, Kalfas A I and Abhari R S 2002 Single pressure transducer probe for 3D flow measurements *The 16th Symp. on Measuring Techniques in Transonic and Supersonic Flow in Cascades and Turbomachines (Cambridge, UK)*
- [10] Gossweiler C R, Kupferschmied P and Gyarmathy G 1995 On fast response probes: part 1. Technology, calibration and application to turbomachinery *ASME J. Turbomach.* **117** 611–7
- [11] Johansen E S and Rediniotis O K 2000 Development of unsteady calibration facilities and techniques for fast-response pressure probes *40th AIAA Aerospace Sciences Meeting and Exhib. (Reno, NV) AIAA paper 2002-0689*

- [12] Treaster A L and Yocum A M 1997 The calibration and application of five-hole probes *ISA Trans.* **18** 23–34
- [13] Pisasale A J and Ahmed N A 2002 Theoretical calibration for highly three-dimensional low-speed flows of a five-hole probe *Meas. Sci. Technol.* **13** 1100–7
- [14] Humm H, Gossweiler C R and Gyarmathy G 1994 On fast-response probes: part 2. Aerodynamic design studies *ASME J. Turbomach.* **117** 618–24
- [15] Kupferschmied P, Köppel P, Gizzi W, Roduner C and Gyarmathy G 2000 Time-resolved flow measurements with fast-response aerodynamic probes in turbomachines *Meas. Sci. Technol.* **11** 1036–54
- [16] Kupferschmied P, Köppel P, Roduner C and Gyarmathy G 2000 On the development and application of the fast-response aerodynamic probe system in turbomachines: part 1. The measurement system *ASME J. Turbomach.* **122** 505–16
- [17] Persico G, Gaetani P and Guardone A 2005 Design and analysis of new concept fast-response pressure probes *Meas. Sci. Technol.* **16** 1741–50
- [18] Tanaka K, Kalfas A I and Hodson H P 2000 Development of single sensor fast response pressure probes *15th Symp. on Measuring Techniques in Transonic and Supersonic Flows in Cascades and Turbomachines (Florence, Italy)*
- [19] Schlienger J, Kalfas A I and Abhari R S 2005 Vortex-wake-blade interaction in a shrouded axial turbine *ASME J. Turbomach.* **127** 699–707
- [20] Denton J D 1993 Loss mechanisms in turbomachines *ASME J. Turbomach.* **115** 621–56
- [21] Sharma O P, Picket G F and Ni R H 1992 Assessment of unsteady flows in turbines *ASME J. Turbomach.* **114** 79–90
- [22] Doorly D J 1988 Modelling the unsteady flow in a turbine passage *ASME J. Turbomach.* **110** 27–37